

Simulating 2+1d \mathbb{Z}_3 lattice gauge theory with iPEPS

Daniel Robaina,¹ Mari Carmen Bañuls,^{1,2} and J. Ignacio Cirac^{1,2}

¹Max-Planck-Institut für Quantenoptik, Hans-Kopfermann-Str. 1, D-85748 Garching, Germany

²Munich Center for Quantum Science and Technology (MCQST), Schellingstr. 4, D-80799 München
(Dated: July 24, 2020)

We simulate a zero-temperature pure \mathbb{Z}_3 Lattice Gauge Theory in 2+1 dimensions by using an iPEPS (Infinite Projected Entangled-Pair State) ansatz for the ground state. Our results are therefore directly valid in the thermodynamic limit. They clearly show two distinct phases separated by a phase transition. We introduce an update strategy that enables plaquette terms and Gauss-law constraints to be applied as sequences of two-body operators. This allows the use of the most up-to-date iPEPS algorithms. From the calculation of spatial Wilson loops we are able to prove the existence of a confined phase. We show that with relatively low computational cost it is possible to reproduce crucial features of gauge theories. We expect that the strategy allows the extension of iPEPS studies to more general LGTs.

Introduction.— For years, Tensor Networks (TN) have been exploited to study quantum many-body problems, especially in the context of condensed matter physics, since they provide efficient ansätze for ground states, low lying excitations and thermal equilibrium states of local hamiltonians [1–5]. The application of TN to Lattice Gauge Theories (LGT) constitutes a much newer, but also fast growing field. Their suitability for 1+1 dimensional problems has already been widely demonstrated using the matrix product state (MPS) ansatz. In numerous studies, MPS have been shown to efficiently and accurately describe the relevant equilibrium physics of abelian and non-abelian LGTs, even at finite density where the infamous sign-problem would turn traditional Monte Carlo approaches infeasible, TN enable continuum limit extrapolations, as well as simulations in out-of-equilibrium scenarios (see [6, 7] for recent reviews).

The one-dimensional success strongly motivates an extension of the TN study to LGT in higher spatial dimensions, where the natural generalization of the MPS ansatz is provided by projected entangled pair states (PEPS) [8], or its infinite version defined directly in the thermodynamic limit, iPEPS [9]. More restricted TN have allowed some first encouraging steps for two dimensional models. Early on, the phase diagram of a \mathbb{Z}_2 LGT was studied with MERA[10, 11], and, more recently, tree tensor networks [12] were applied to explore the $U(1)$ quantum link model on a finite lattice [13]. But a fully variational PEPS calculation for a LGT does not yet exist.

Although the fast progress in iPEPS algorithms has allowed reaching some of the most competitive results for certain condensed matter problems [14–20] and there is no conceptual limitation to apply them to LGTs [21], until the date the only numerical results of (i)PEPS simulations of LGTs have been limited to toy models without an actual optimization of the most general tensors [22–26]. Apart from the obvious increase in computational cost, another more limiting factor is the presence of plaquette terms in the LGT Hamiltonian. While it is possible to directly apply a plaquette term to PEPS [27, 28], this in-

volves a considerably higher computational cost than the two-body interactions for which the most efficient PEPS algorithms are optimized, and ultimately limits the bond dimension that can be explored to only very small values, not enough to approach convergence.

In this work we develop a new update strategy that allows the standard plaquette term of a LGT to be applied as a sequence of purely two-body operations. This allows us to use an iPEPS ansatz to study the phase diagram of a \mathbb{Z}_3 -invariant LGT in two spatial dimensions. In agreement to predictions in the literature [29–31], we observe a confining and a non-confining phase. We are able to quantitatively locate the transition at a value of the coupling constant $g_c^2 = 1.159(4)$. This constitutes the first ab initio iPEPS study of a 2+1d Lattice Gauge Theory, and opens the door to studying a rich variety of LGTs using the most efficient up-to-date PEPS algorithms.

Model.— We consider a \mathbb{Z}_3 invariant Lattice Gauge Theory given by the following Hamiltonian in 2+1 space-time dimensions

$$H = H_E + H_\square, \quad (1)$$

where

$$H_E = \frac{g^2}{2} \sum_{\mathbf{x}} E^2(\mathbf{x} + \mathbf{i}/2) + E^2(\mathbf{x} + \mathbf{j}/2)$$

$$H_\square = -\frac{1}{2g^2} \sum_{\mathbf{x}} U_P(\mathbf{x}) + U_P^\dagger(\mathbf{x}).$$

The plaquette operator is written as

$$U_P(\mathbf{x}) = U^\dagger(\mathbf{x} + \mathbf{j}/2) U^\dagger(\mathbf{x} + \mathbf{i}/2 + \mathbf{j}) U(\mathbf{x} + \mathbf{i} + \mathbf{j}/2) U(\mathbf{x} + \mathbf{i}/2)$$

where \mathbf{x} is the position of a vertex and \mathbf{i}, \mathbf{j} are unit-vectors in both space directions connecting two adjacent vertices.

The physical degrees of freedom are the link variables which have a local Hilbert space of dimension $d = 3$ and consequently E takes values in $\{-1, 0, 1\}$. The unitary

operators U and U^\dagger , lower and raise respectively the electric field at the corresponding link by one unit

$$\begin{aligned} U|e\rangle &= |e-1\rangle \\ U^\dagger|e\rangle &= |e+1\rangle \end{aligned}$$

and \mathbb{Z}_3 -symmetry implies $U^3 = (U^\dagger)^3 = \mathbb{1}$.

In the limit of $d \rightarrow \infty$ this \mathbb{Z}_d Hamiltonian yields a $U(1)$ Lattice Gauge Theory where H_E corresponds to the electric field and the plaquette terms in H_\square reproduce the magnetic parts [32].

The Hamiltonian in (1) commutes with the Gauss-law operator $G(\mathbf{x})$ at every point in space giving rise to a local \mathbb{Z}_3 gauge symmetry where $G(\mathbf{x})$ is given by

$$G(\mathbf{x}) = e^{\frac{2\pi i}{3}(E_l(\mathbf{x})+E_d(\mathbf{x})-E_r(\mathbf{x})-E_u(\mathbf{x}))} \quad (2)$$

where the subscripts l, d, r, u correspond to the links which are to the *left, down, right, up* of the vertex at position \mathbf{x} . Notice that $G(\mathbf{x})$ is defined at the vertices of the lattice while the links live inbetween vertices. Given that $[G(\mathbf{x}), H] = 0$, the hamiltonian is block diagonal and physical states that satisfy the Gauss-law obey

$$G(\mathbf{x})|\psi\rangle = e^{\frac{2\pi i}{3}q(\mathbf{x})}|\psi\rangle, \quad (3)$$

where $q(\mathbf{x}) \in \{-1, 0, 1\}$ can be thought of as the static charge at vertex \mathbf{x} . Although the ground state of the system lives in the charge sector with $q(\mathbf{x}) = 0, \forall \mathbf{x}$, it is also interesting to study different charge patterns, as we will do.

Method.— An iPEPS ansatz consists of a unit-cell of rank-5 tensors arranged in a 2D-grid which is repeated in both space directions infinitely many times. Those tensors have a physical index of dimension d equal to that of the local Hilbert space of each degree of freedom (3 in our case) and 4 additional virtual indices of bond dimension D that allow for the interactions with neighbouring tensors. As D increases the ansatz becomes more general and, consequently, a better description of the true quantum state is expected.

There are several ways of optimizing the tensors within the unit-cell in order to find the ground state. One possibility relies on a variational approach in which only one tensor is varied at a time by keeping the rest fixed. The optimal tensor is then found by solving a Generalized Eigenvalue Problem before moving to the next one [2]. While the variational method has been able to obtain very accurate energies [15, 16], the most widely used strategy for iPEPS, which we also adopt here, is still an imaginary time evolution, very much in the spirit of the popular Time Evolving Block Decimation (TEBD) algorithm [33]. In the most efficient version, a simple update (SU) [34] strategy is used to find the optimized tensors.

We use a second order Suzuki-Trotter [35, 36] expansion of the Hamiltonian exponential

$$e^{-\beta(H_E+H_\square)} = \lim_{n \rightarrow \infty} \left(e^{-\frac{\delta\tau}{2}H_E} e^{-\delta\tau H_\square} e^{-\frac{\delta\tau}{2}H_E} \right)^n \quad (4)$$

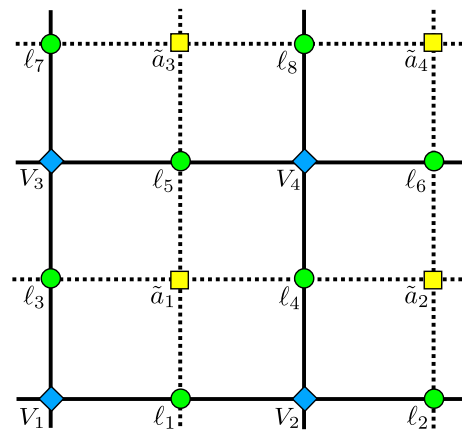


FIG. 1. iPEPS unit-cell.

with $\delta\tau = \beta/n$ and β the total imaginary time evolved until convergence.

Traditional iPEPS algorithms have been optimized for Hamiltonians with nearest neighbor interactions. Longer range or higher-order terms considerably increase the computational cost. Therefore, in order to apply these methods to our problem, we need a simple and efficient update strategy that takes into account 4-body plaquette operators like the ones that appear in LGTs.

In order to apply the plaquette operator in its exponential form we import an idea originally envisioned for digital quantum simulations of LGTs [37–40]. The key aspect consists in including an auxiliary degree of freedom with the same Hilbert space as the links themselves at the center of each plaquette. This ancilla is prepared in a state which is an equal weight symmetric superposition of all basis states. Following the notation of [38] we call it $|\tilde{\text{in}}\rangle = \frac{1}{\sqrt{3}} \sum_{m=-1,0,1} |\tilde{m}\rangle$. The derivation presented in the above mentioned papers allows us to write the action of the four-body operator $e^{-\delta\tau H_\square}$ as a sequence of two-body gates (we call this the *entangler*) followed by a local operation on the ancilla. The inverse of the entangler (the *disentangler*) leaves the ancilla back in its original state $|\tilde{\text{in}}\rangle$, ready for the next update. The full identity reads

$$\mathcal{U}_\square^\dagger e^{\frac{\delta\tau}{2g^2}(\tilde{U}+\tilde{U}^\dagger)} \mathcal{U}_\square |\tilde{\text{in}}\rangle = |\tilde{\text{in}}\rangle e^{-\delta\tau H_\square} \quad (5)$$

where the entangler $\mathcal{U}_\square = \mathcal{U}_l^\dagger \mathcal{U}_u^\dagger \mathcal{U}_r \mathcal{U}_d$ is the product of four two-body gates between ancilla and the corresponding links. Each of these two-body gates is written as

$$U_i = U_i \otimes \tilde{P}_1 + \mathbb{1}_i \otimes \tilde{P}_0 + U_i^\dagger \otimes \tilde{P}_{-1} \quad (6)$$

where U_i with $i = l, u, r, d$ act on the links and \tilde{P}_m are ordinary projectors in the ancilla Hilbert space that project onto state $|\tilde{m}\rangle$. The local operation on the ancilla $e^{\frac{\delta\tau}{2g^2}(\tilde{U}+\tilde{U}^\dagger)}$ involves \tilde{U} and \tilde{U}^\dagger which are nothing but ordinary U (and U^\dagger)-operators acting on the ancilla degrees

of freedom. Note, that (5) is a mathematical identity and there is no approximation involved. We refer the interested reader to the original papers for a clean derivation of (5).

The electrical evolution corresponds to a sequential action of $e^{-\frac{\delta\tau g^2}{4} E^2}$ -single-site operators onto the physical indices of all links. Since we employ the simple update procedure (SU) this operation does not increase the bond dimensions and thus carries no truncation errors.

In order to implement the update procedure described above, we choose a 4×4 unit cell as our iPEPS ansatz as shown in Fig. 1. The unit cell contains 16 different tensors, 8 of them corresponding to the gauge degrees of freedom residing on the links (green circles labelled ℓ_i , with $i = 1, \dots, 8$), plus four tensors for the ancillas (yellow squares) at the center of the plaquettes and four for the vertices (blue diamonds). The solid lines represent the physical lattice of the system that connects links and vertices while the dashed lines correspond to an auxiliary lattice that connects ancillas with links.

iPEPS are able to account for global and local symmetries of the theory by imposing a particular block structure of the tensors [22–24, 41–44]. In our case, this is ensured by applying a gauge projector that enforces the Gauss-law on the vertices [45]. Since all the terms in the Hamiltonian commute with $G(\mathbf{x})$, it is enough to apply the projector at the beginning of the imaginary time evolution. To cope with potential errors introduced by the truncation, we subsequently monitor the expectation value of $G(\mathbf{x})$ to be sure to stay in the sector of interest. We observe that the deviation (with respect to the desired sector) is not larger than 10^{-6} in any of our simulations.

Similarly to other Tensor Networks, iPEPS allow for the calculation of local observables. This requires an accurate approximation of the environment around a given tensor. In this work we calculate the environment with the Corner Transfer Matrix (CTM)-method [46, 47], which introduces an additional bond dimension, controlling the precision of such approximation [48].

Altogether, this strategy allows us to simulate the imaginary time evolution of a LGT including the four-body plaquette operator by means of well-known tools to the iPEPS practitioners like single and two-body gates.

Phase Diagram.— When $g^2 \rightarrow \infty$, the electric field term dominates and, in the case of vanishing static charges at all the vertices, the lowest energy is attained when all links are in the zero electric flux state. The ground state thus becomes a product state with zero energy. Similarly, in the weak coupling regime when $g^2 \rightarrow 0$ the energy per plaquette tends towards the asymptotic value of $-1/g^2$ where the ground state is again a product state. It is well known that \mathbb{Z}_d gauge theories are dual to spin systems with nearest neighbour interactions [29]. For \mathbb{Z}_3 in $2 + 1$ dimensions the system undergoes a

first order phase transition [30, 31] around some critical coupling g_c^2 .

We have performed calculations at $D = 3, 4, 5$ for the whole range of couplings from $g^2 = 0.01$ to $g^2 = 5.0$. As expected, increasing the bond dimension yields lower energies in general. We observe that for some values of the coupling constant near the phase transition, $D = 5$ was not able to provide a lower estimate than $D = 4$. We attribute this to a lack of full convergence of the SU on those points. Since for the rest of parameters the relative difference between the results for $D = 4$ and 5 is extremely small (see SM), we take $D = 4$ as our best data-set and use $D = 3$ and 5 to estimate numerical errors [49]. Our ground-state energy results are plotted in Fig. 2.

First order phase transitions can be cleanly detected by TN simulations [50] as cusps in the energy curve, corresponding to a level crossing. This effect is apparent in Fig. 2 at intermediate values of the coupling (the dashed lines are meant to guide the eye). A cleaner way of locating the phase transition is by the discontinuity in the first derivative of the energy, which can be calculated as

$$\frac{\partial E_0^{q(\mathbf{x})=0}}{\partial g^2} = \langle \psi_{\text{GS}} | \frac{\partial H}{\partial g^2} | \psi_{\text{GS}} \rangle = \frac{1}{g^2} \langle \psi_{\text{GS}} | H_{\text{E}} - H_{\square} | \psi_{\text{GS}} \rangle \quad (7)$$

and is plotted in Fig. 3. A clear discontinuity between $g_c^2 = 1.15$ and $g_c^2 = 1.175$ can be identified.

We also consider a different charge sector, in which we project two adjacent vertices to static charges 1 and -1 respectively (as illustrated in Fig. 5). Below the phase transition, both sectors are close to degenerate (see Fig. 2), and as soon the transition is crossed, they separate. The energy per plaquette of the static charges tends to $g^2/8$ in the limit of $g^2 \rightarrow \infty$ since our unit cell contains 4 plaquettes and in that limit there is a single link whose E^2 -expectation value is 1, while the rest vanish. The fact that the energies of both sectors start to strongly deviate from each other exactly at the phase transition represents a consistency check that we have correctly located the transition region. We will attempt a more accurate determination of g_c^2 via Wilson loops in the following section.

Wilson loops.— The phase transition separates a non-confining (for small g^2) from a confining (for large g^2) phase. We can characterize it by investigating the ground state expectation value of several closed spatial Wilson loops, the simplest of them being the plaquette which enters the calculation of the energy. In the confining phase, these values are expected to decay exponentially with the area of the loop. Due to the large computational cost of these quantities, we restrict ourselves to loops of width 1 and length $n = 1, \dots, 6$. The corresponding operator can be written in closed form as

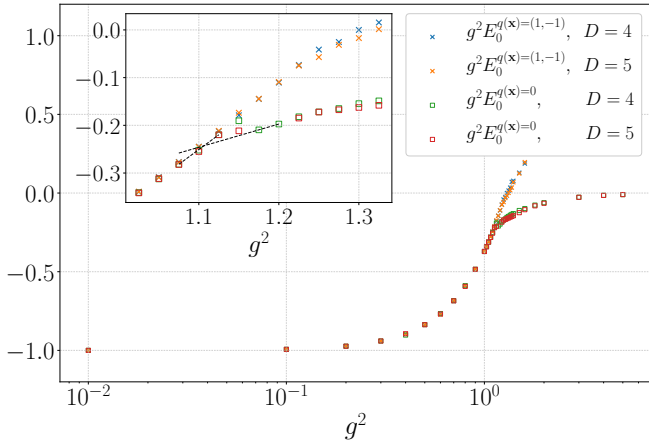


FIG. 2. Ground State Energies for the zero charge sector with bond dimensions $D = 4, 5$. We compare to the sector of two adjacent vertices respectively projected to charges 1 and -1 with bond dimension $D = 4, 5$. Inset: Transition region zoom in.

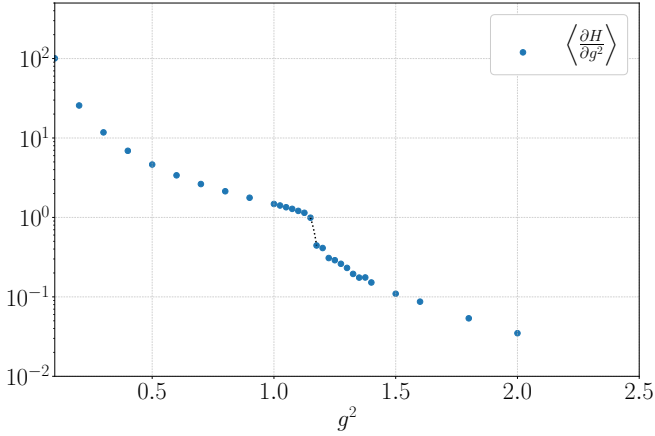


FIG. 3. Expectation value of $\frac{\partial H}{\partial g^2}$ on the ground state for the zero charge sector. Bond dimension is $D = 4$.

$$W_{1 \times n} = U^\dagger(\mathbf{x} + \mathbf{j}/2) \otimes \left(\bigotimes_{\alpha=0}^{n-1} U(\mathbf{x} + (\alpha + 1/2)\mathbf{i}) \right) \otimes U(\mathbf{x} + n\mathbf{i} + \mathbf{j}/2) \otimes \left(\bigotimes_{\beta=0}^{n-1} U^\dagger(\mathbf{x} + (n - \beta - 1/2)\mathbf{i} + \mathbf{j}) \right). \quad (8)$$

We calculate $\langle \psi_{\text{GS}} | W_{1 \times n} | \psi_{\text{GS}} \rangle$ and show the results in figure 4. We perform a linear fit of the logarithm of the real part of $\langle W_{1 \times n} \rangle$ (the imaginary part is consistent with zero) vs. the area n , and read off the slope σ . The phase transition clearly manifests in a sudden increase of σ when the coupling approaches a critical value g_c^2 . In order to extract this critical value, we perform several fits of the data to a form $A(g^2 - g_c^2)^\alpha$ and estimate the errors

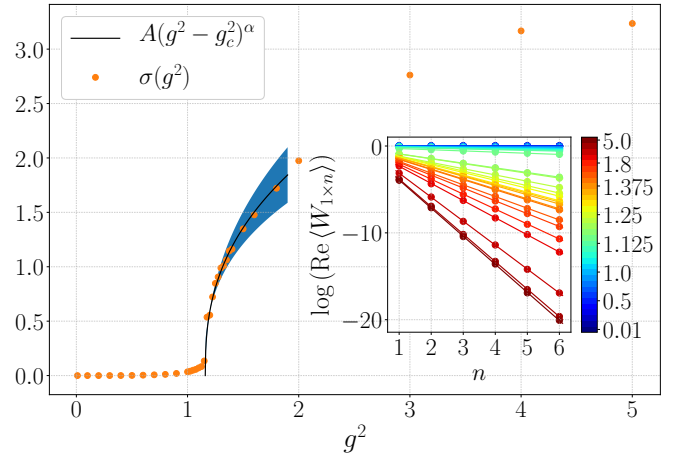


FIG. 4. Area-law coefficient σ obtained from the fit of the expectation value of the Wilson loops that is shown in the inset for $D = 4$ ground states. The colorbar represents the value of the coupling g^2 . The blue band represents an error estimation for the fitted curve.

by varying the number of points included in the fit. We find

$$A = 2.0(3), \quad g_c^2 = 1.159(4), \quad \alpha = 0.39(3). \quad (9)$$

Electric field map.— In order to illustrate clearly the very different behavior of the electric field in both phases, in figure 5 we plot $\langle \psi_{\text{GS}} | E_\ell^2 | \psi_{\text{GS}} \rangle$ for all 8 links in the unit-cell in different charge sectors. The zero charge sector keeps translational symmetry for all values of the coupling and above the phase transition the electric field is practically zero. For the case of two static charges, we see that below the phase transition the behavior is very similar as in the zero charge sector, while as soon as the transition is crossed, the electric field is confined to a single link between two charges.

Conclusions.— We find that iPEPS are capable of accurately capturing the Physics of a gauge theory with different phases in 2+1 space-time dimensions. With moderate bond dimension, the iPEPS ansatz allows us not only to determine the ground state energy but also to explore the phenomenology of the model, including the location of a confinement phase transition.

Key to this development is a special update strategy that employs additional ancillary degrees of freedom and reduces many-body terms to sequences of two-body operations. This allows us to deal with plaquette terms in an efficient way, and also to correctly implement Gauss-law constraints at the vertices as a way to impose the local symmetry.

The strategy can be immediately applied to other LGTs, but also to other hamiltonians that require the inclusion of a 4-body operator. Since the original construction [40] on which this update is based can be applied to non-Abelian Lie groups and also to operators

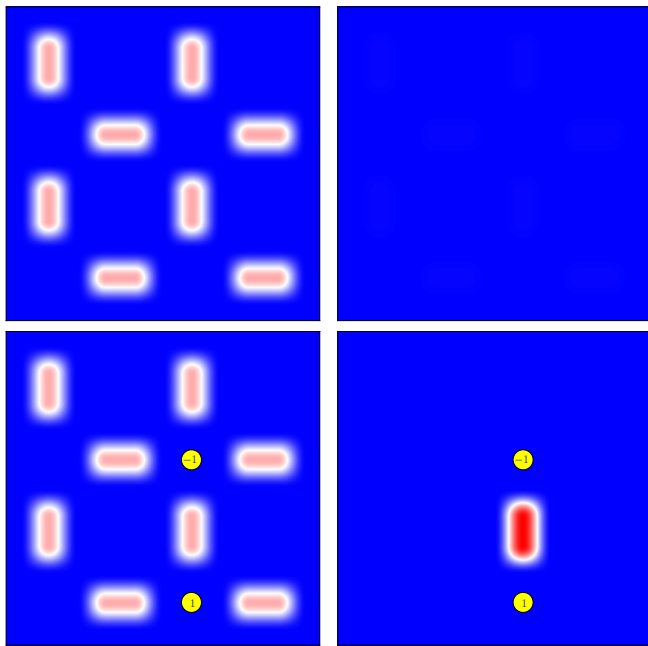


FIG. 5. Ground state expectation values of E^2 -operators acting on the links of the unit-cell for $g^2 = 0.01, 5.0$. The upper row corresponds to the zero static charge sector while the lower has two vertices (yellow circles) projected to 1 and -1 static charges.

acting on a larger number of sites [39, 51], we expect that the method can be further generalized. Dynamical fermions can additionally be included in the approach without involving a sign-problem, and we leave this direction for future work. Altogether, this opens the door to more ambitious iPEPS studies of LGTs.

We thank Claudius Hubig for insightful discussions on the SyTen toolkit used in this work [52, 53]. This work was partly supported by the Deutsche Forschungsgemeinschaft (DFG, German Research Foundation) under Germany's Excellence Strategy – EXC-2111 – 390814868, and EU-QUANTERA project QTFLAG (BMBF grant No. 13N14780).

[1] J. I. Cirac and F. Verstraete, *Journal of Physics A: Mathematical and Theoretical* **42**, 504004 (2009).
 [2] F. Verstraete, V. Murg, and J. Cirac, *Adv. Phys.* **57**, 143 (2008).
 [3] U. Schollwöck, *Ann. Phys.* **326**, 96 (2011), january 2011 Special Issue.
 [4] R. Orús, *Annals Phys.* **349**, 117 (2014), arXiv:1306.2164 [cond-mat.str-el].
 [5] P. Silvi, F. Tschirsich, M. Gerster, J. Jünemann, D. Jaschke, M. Rizzi, and S. Montangero, *SciPost Phys. Lect. Notes*, 8 (2019).
 [6] M. C. Bañuls and K. Cichy, *Rept. Prog. Phys.* **83**, 024401 (2020), arXiv:1910.00257 [hep-lat].

[7] M. C. Bañuls, R. Blatt, J. Catani, A. Celi, J. I. Cirac, M. Dalmonte, L. Fallani, K. Jansen, M. Lewenstein, S. Montangero, C. A. Muschik, B. Reznik, E. Rico, L. Tagliacozzo, K. Van Acoleyen, F. Verstraete, U. J. Wiese, M. Wingate, J. Zakrzewski, and P. Zoller, arXiv e-prints, arXiv:1911.00003 (2019), arXiv:1911.00003 [quant-ph].
 [8] F. Verstraete and J. Cirac, (2004), arXiv:cond-mat/0407066.
 [9] J. Jordan, R. Orús, G. Vidal, F. Verstraete, and J. I. Cirac, *Phys. Rev. Lett.* **101**, 250602 (2008).
 [10] G. Vidal, *Phys. Rev. Lett.* **99**, 220405 (2007).
 [11] L. Tagliacozzo and G. Vidal, *Phys. Rev. B* **83**, 115127 (2011), arxiv:1007.4145.
 [12] Y.-Y. Shi, L.-M. Duan, and G. Vidal, *Phys. Rev. A* **74**, 022320 (2006).
 [13] T. Felser, P. Silvi, M. Collura, and S. Montangero, “Two-dimensional quantum-link lattice quantum electrodynamics at finite density,” (2019).
 [14] P. Corboz, *Phys. Rev. B* **93**, 045116 (2016).
 [15] P. Corboz, *Phys. Rev. B* **94**, 035133 (2016).
 [16] L. Vanderstraeten, J. Haegeman, P. Corboz, and F. Verstraete, *Phys. Rev. B* **94**, 155123 (2016).
 [17] P. Corboz, P. Czarnik, G. Kapteijns, and L. Tagliacozzo, *Phys. Rev. X* **8**, 031031 (2018).
 [18] M. Rader and A. M. Läuchli, *Phys. Rev. X* **8**, 031030 (2018).
 [19] L. Vanderstraeten, J. Haegeman, and F. Verstraete, *Phys. Rev. B* **99**, 165121 (2019).
 [20] C. Hubig and J. I. Cirac, *SciPost Phys.* **6**, 31 (2019).
 [21] K. Zapp and R. Orús, *Phys. Rev. D* **95**, 114508 (2017).
 [22] L. Tagliacozzo, A. Celi, and M. Lewenstein, *Phys. Rev. X* **4**, 041024 (2014).
 [23] E. Zohar, M. Burrello, T. B. Wahl, and J. I. Cirac, *Ann. Phys. (Amsterdam)* **363**, 385 (2015).
 [24] J. Haegeman, K. Van Acoleyen, N. Schuch, J. I. Cirac, and F. Verstraete, *Phys. Rev. X* **5**, 011024 (2015).
 [25] E. Zohar, T. B. Wahl, M. Burrello, and J. I. Cirac, *Annals Phys.* **374**, 84 (2016), arXiv:1607.08115 [quant-ph].
 [26] E. Zohar and J. I. Cirac, *Phys. Rev. D* **97**, 034510 (2018).
 [27] S. Dusuel, M. Kamfor, R. Orús, K. P. Schmidt, and J. Vidal, *Phys. Rev. Lett.* **106**, 107203 (2011).
 [28] M. D. Schulz, S. Dusuel, R. Orús, J. Vidal, and K. P. Schmidt, *New Journal of Physics* **14**, 025005 (2012).
 [29] C. P. K. Altes, *Nuclear Physics B* **142**, 315 (1978).
 [30] H. W. J. Blöte and R. H. Swendsen, *Phys. Rev. Lett.* **43**, 799 (1979).
 [31] G. Bhanot and M. Creutz, *Phys. Rev. D* **21**, 2892 (1980).
 [32] The limit of $U(1)$ is recovered when $d \rightarrow \infty$ if the Hamiltonian is written in the form of [?] but for $d = 3$ our formulation is equivalent except for a trivial rescaling of g^2 and the U operator and a constant overall shift in the Hamiltonian.
 [33] G. Vidal, *Phys. Rev. Lett.* **91**, 147902 (2003).
 [34] H. C. Jiang, Z. Y. Weng, and T. Xiang, *Phys. Rev. Lett.* **101**, 090603 (2008).
 [35] H. F. Trotter, *Proc. Amer. Math. Soc.* **10**, 545 (1959).
 [36] M. Suzuki, *Journal of Mathematical Physics* **26**, 601 (1985).
 [37] E. Zohar, A. Farace, B. Reznik, and J. I. Cirac, *Phys. Rev. Lett.* **118**, 070501 (2017), arXiv:1607.03656 [quant-ph].
 [38] E. Zohar, A. Farace, B. Reznik, and J. I. Cirac, *Phys.*

- Rev. **A95**, 023604 (2017), arXiv:1607.08121 [quant-ph].
- [39] E. Zohar, J. Phys. **A50**, 085301 (2017), arXiv:1607.08122 [quant-ph].
- [40] J. Bender, E. Zohar, A. Farace, and J. I. Cirac, New J. Phys. **20**, 093001 (2018), arXiv:1804.02082 [quant-ph].
- [41] D. Pérez-García, M. M. Wolf, M. Sanz, F. Verstraete, and J. I. Cirac, Phys. Rev. Lett. **100**, 167202 (2008).
- [42] S. Singh, R. N. C. Pfeifer, and G. Vidal, Phys. Rev. A **82**, 050301 (2010).
- [43] D. Pérez-García, M. Sanz, C. E. González-Guillén, M. M. Wolf, and J. I. Cirac, New Journal of Physics **12**, 025010 (2010).
- [44] E. Zohar and M. Burrello, New J. Phys. **18**, 043008 (2016).
- [45] See the Supp. Mat. for more details on the projection.
- [46] R. Orús and G. Vidal, Phys. Rev. B **80**, 094403 (2009).
- [47] P. Corboz, J. Jordan, and G. Vidal, Phys. Rev. B **82**, 245119 (2010).
- [48] An error analysis on the convergence of the CTM can be found in the Supp. Mat.
- [49] See Supp. Mat. for an error estimate on our data.
- [50] R. Orús, A. C. Doherty, and G. Vidal, Phys. Rev. Lett. **102**, 077203 (2009).
- [51] E. Zohar, Phys. Rev. D **101**, 034518 (2020).
- [52] “The SYTEN toolkit,” .
- [53] C. Hubig, *Symmetry-Protected Tensor Networks*, Ph.D. thesis, LMU München (2017).

SUPPLEMENTARY MATERIAL

Gauss-Law Constrains

In order to enforce the Gauss-Law at every vertex, we define the projector

$$P_q(\mathbf{x}) = \frac{1}{3} \sum_{n=-1,0,1} \left(e^{\frac{2\pi i}{3}(E_l(\mathbf{x})+E_d(\mathbf{x})-E_r(\mathbf{x})-E_u(\mathbf{x})-q(\mathbf{x}))} \right)^n \quad (10)$$

which projects vertex \mathbf{x} to charge $q(\mathbf{x})$. Since E -field operators in the exponent commute with each other, this projector has the same structure as H_{\square} since it can be written as a product of four single-site operators. Taking $q(\mathbf{x}) = 0$ as an example case, it is convenient to consider a slight modification of identity (5)

$$\mathcal{G}^\dagger \frac{1}{3} \left(\tilde{\mathbb{1}} + \tilde{U} + \tilde{U}^\dagger \right) \mathcal{G} |\tilde{\text{in}}\rangle = |\tilde{\text{in}}\rangle P_0 \quad (11)$$

where now the entangler between vertex \mathbf{x} and the links surrounding it can be again written as a sequence of four two-body gates $\mathcal{G} = \mathcal{G}_l \mathcal{G}_d \mathcal{G}_r^\dagger \mathcal{G}_u^\dagger$. Each of the two-body gates is written as

$$\mathcal{G}_i = g_i \otimes \tilde{P}_1 + \mathbb{1}_i \otimes \tilde{P}_0 + g_i^\dagger \otimes \tilde{P}_{-1} \quad (12)$$

with $g_i = e^{\frac{2\pi i}{3} E_i(\mathbf{x})}$ and $i = l, u, r, d$. Similarly to the case with the ancillas, (11) is only true if vertex tensors are initialized in their $|\tilde{\text{in}}\rangle$ states. In this way, enforcing the Gauss-law at every vertex is as simple as applying a sequence of single and two-body gates. Only a minor modification to the local operation $\frac{1}{3} \left(\tilde{\mathbb{1}} + \tilde{U} + \tilde{U}^\dagger \right)$ on the vertex allows us to also obtain $P_q(\mathbf{x})$ with $q(\mathbf{x}) = \pm 1$.

Errors

The left plot in Fig. 6 shows for different values of the couplings our results for the ground state energy for different values of the bond dimension. It can be seen that at weak coupling the error is negligible. In fact, the difference between $D = 4$ and $D = 5$ is less than 10^{-9} . This is not surprising, since the true ground state tends to a product state for $g^2 \rightarrow 0$. At intermediate couplings and near the phase transition the error rises up to 6% and stays rather constant up to strong couplings where the signal is so weak that round-off errors start to become an issue.

When calculating expectation values via the CTM-method, it is crucial to ensure that the approximation of the environment has converged. To this end, it is customary to repeat the calculation of local observables with different number of states χ included in the environment. The right plot in Fig. 6 shows for the case of $D = 4$ the ground state energy from $\chi = 1$ up to $\chi = 32$.

Another convergence test can be performed at fixed value of χ by monitoring the change in expectation values as we keep absorbing unit-cells into the environment tensors. We have set 10^{-6} as the acceptable threshold for the difference in between iterations (see Fig. 7). From these analysis we can conclude that the error is dominated by the bond dimension D of the state.

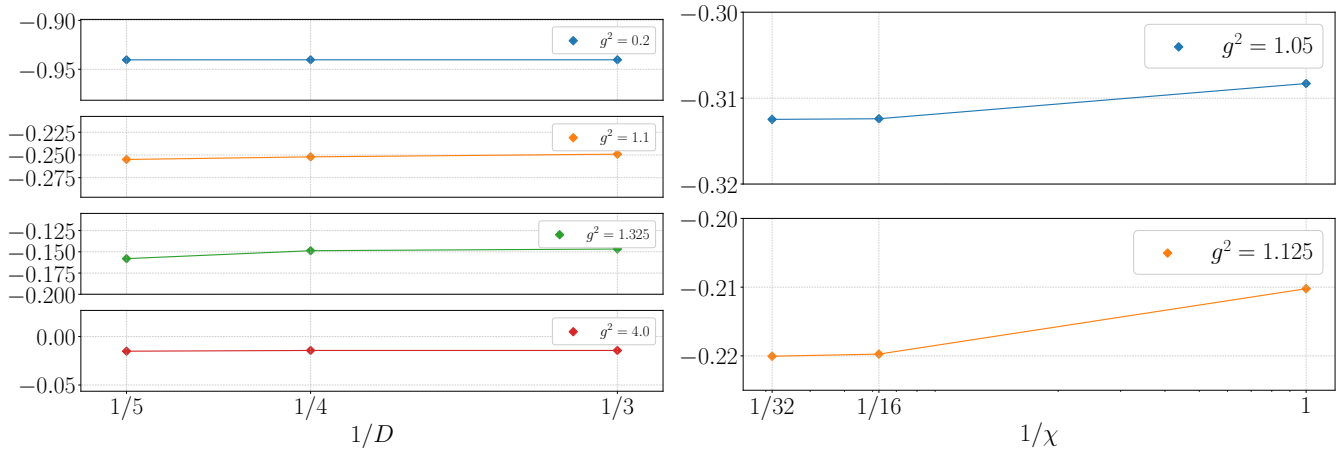


FIG. 6. Left: Ground state Energies $g^2 E_0$ for the zero charge sector for different bond dimensions ($D = 3, 4, 5$). Right: Same quantity as a function of the number of states χ included in the CTM.

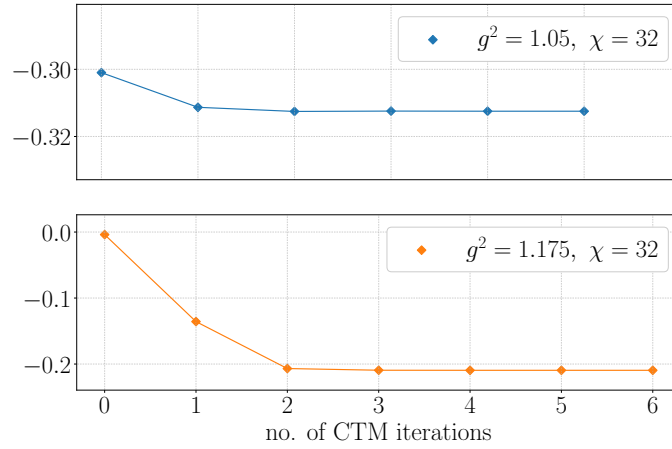


FIG. 7. Ground state Energies $g^2 E_0$ for $\chi = 32$ and $D = 4$ as function of CTM-iterations.